Int. J. Heat Mass Transfer. Vol. 32, No. 12, pp. 2459–2474, 1989
Printed in Great Britain

0017–9310/89 $3.00 + 0.00

A comparison of the flow boiling performance characteristics of partially-heated cross-ribbed channels with different rib geometries

M. COHEN and V. P. CAREY
Department of Mechanical Engineering, University of California, Berkeley, CA 94720, U.S.A.

(*Received* 14 *June* 1988 *and in final form* 7 *April* 1989)

Abstract—Measured local heat transfer data and the results of flow visualization experiments are reported for convective boiling of R-113 and methanol in vertical cross-ribbed channels similar to geometries used in formed-plate compact heat exchangers. Experiments are conducted using a test section in which one wall of the channel is heated while the opposite wall is adiabatic and transparent to allow visual observation of the flow. Heat transfer data are obtained for three different rib crossing patterns at coolant mass flux values between 40 and 230 kg m^{-2} s^{-1} and mass qualities between 0.10 and 0.80. Comparison of these data, together with those for a fourth geometry previously reported, indicate that variations of the rib spacing and angle have a significant effect on boiling heat transfer performance. Variation of the rib crossing pattern in these channels is found to have only a small effect on heat transfer. The swirl and agitation induced by the ribs are found to increase the convective boiling heat transfer coefficient by as much as a factor of 4 above that for a round tube under comparable flow conditions. Methods of correlating the heat transfer data for annular film-flow boiling in these geometries are also discussed.

INTRODUCTION

FORMED-plate heat exchangers having cross-ribbed channel geometries have been widely used in the chemical and food processing industries and in aerospace and automotive applications for many years. Most often, these units are used for single-phase heat transfer applications. However, units of this type have also seen limited use as evaporators in process heat transfer applications in the chemical and petroleum industries. Various types of ribbed-plate channels have also been used in compact brazed aluminum evaporators for automotive air conditioning systems.

Despite their use in the applications noted above, available information on convective boiling and two-phase flow in cross-ribbed channel geometries is very limited. The flow boiling heat transfer performance of several different ribbed-plate heat exchangers was determined experimentally in a recent study by Panchal *et al.* [1]. Ribbed-plate heat exchangers manufactured by Tranter and Alpha-Laval were tested with the channels oriented vertically with ammonia or R-12 as the working fluid. Overall heat transfer performance of these units was reported, but the heat transfer coefficient on the evaporating side (either local or mean) cannot be determined from these data.

In a more recent study, Xu and Carey [2] experimentally investigated the flow boiling heat transfer in a partially-heated channel with cross-ribbed walls. A special test section was used in this study which permitted direct visual observation of the boiling process while simultaneously measuring local heat transfer coefficients at several locations along the channel. Heat transfer data were obtained for wide ranges of mass flux and quality using water, methanol or n-butanol as coolants.

For the cross-ribbed channel geometry tested by Xu and Carey [2], a rapid transition to an annular flow configuration was observed during vertical flow boiling in the channel. Although nucleate boiling appeared to be almost completely suppressed a short distance downstream of the onset of saturated boiling, the measured boiling heat transfer coefficients were typically two to three times greater than values predicted by correlations for round tubes under comparable conditions. Partial dryout of the surface was observed at high qualities which resulted in a drop in the heat transfer coefficient.

A recent paper by Ohara and Takahashi [3] summarizes the results of a study of flow boiling of R-12 in a Nippondensu compact evaporator having formed-plate tubes with cross-ribbed walls. These investigators used a fiber-optic probe to investigate the two-phase flow characteristics in the cross-ribbed channel. Although some convective boiling heat transfer data are also presented, the corresponding tube wall temperatures and flow conditions are not provided, which makes interpretation of the results somewhat difficult. However, the sequence of flow regimes and the variation of the heat transfer coefficient as the quality increases are qualitatively identical to those observed by Xu and Carey [2].

Another recent paper by Marseille *et al.* [4] summarizes experiments in which localized heat transfer

NOMENCLATURE

A	constant in equation (6)
A_0	cross sectional open area of channel
A_P	primary surface area in channel section of length L_c
A_R	surface area of ribs in channel section of length L_c
c_P	specific heat at constant pressure
d_h	hydraulic diameter based on wetted perimeter, $4A_0/P_W$
d_{hp}	hydraulic diameter based on heated perimeter, $4A_0/P_H$
f	friction factor
F	convective boiling parameter, $(h_c/h_{fp})\ Pr_f^{-0.296}$
G	mass flux
h_{tp}	two-phase heat transfer coefficient
h_c	forced convective evaporation component of h_{tp}
h_{fp}	single-phase liquid heat transfer coefficient for the partially-heated channel
h_{fg}	latent heat of vaporization of coolant
H	dimension of ribs from root to tip
j	Colburn j factor, $St_{fp}\ Pr_f^{2/3}$
j_f	volume flux of liquid, $G(1-x)/\rho_f$
j_g	volume flux of vapor, Gx/ρ_g
k_c	conductivity of copper
L_c	length of channel section
n	exponent in equation (6)
p	pressure
P_H	heated perimeter
P_W	wetted perimeter
Pr_f	liquid Prandtl number
Re_f	liquid Reynolds number, $G(1-x)d_h/\mu_f$
Re_{fp}	liquid Reynolds number based on heated perimeter, $G(1-x)d_{hp}/\mu_f$
Re_g	vapor Reynolds number, Gxd_h/μ_g
St	Stanton number, h/Gc_P
t	rib thickness
T_c	temperature in copper slab
T_M	bulk mean temperature of the coolant
T_w	wall temperature of primary surface of channel
T_{sat}	saturation temperature of coolant
W_c	width of copper slab
x	mass quality
X_{tt}	Martinelli parameter for turbulent–turbulent flow, $[(dp/dz)_{Ff}/(dp/dz)_{Fg}]^{1/2}$.

Greek symbols

η_R	rib fin efficiency
μ	absolute viscosity
ρ	density
Ψ	parameter defined in equation (3).

Subscripts

f	liquid properties or corresponding to liquid flow alone in the channel
fp	liquid flow alone in the partially-heated channel
F	friction component of pressure gradient
g	vapor properties or corresponding to vapor flow alone in the channel
tp	two-phase flow conditions.

coefficients for convective boiling of R-12 inside the ribbed-plate passages of a compact evaporator were determined from full-core tests. In these experiments the ribbed channels were oriented horizontally. The data obtained in this study indicate that the heat transfer coefficient first increases with increasing quality (and downstream distance), peaking at about 50% quality, and then decreases towards the value for pure vapor flow. This trend in the heat transfer coefficient data is identical to that observed in the partially-heated single channel experiments of Xu and Carey [2]. Based on this similarity in the results of these two studies, Marseille *et al.* [4] concluded that the peaking and roll-over of the heat transfer coefficient with increasing quality was associated with the progressive dryout of the tube wall observed directly by Xu and Carey [2].

Although the studies of Xu and Carey [2], Ohara and Takahashi [3], and Marseille *et al.* [4] provide considerable insight into the nature of flow boiling heat transfer in cross-ribbed channels, there are aspects of the transport for these circumstances which still are not well understood. In particular, the effects of varying the rib geometry and spacing is still largely unexplored. More information about the effects of changing the geometry would make it possible to more fully assess the advantages of using ribbed-plate geometries for evaporator applications.

In the study summarized here, the flow boiling characteristics of three different cross-ribbed channel geometries were determined experimentally in an effort to explore the effects of rib geometry variations on two-phase transport. Experiments were conducted using a test section similar to that used by Xu and Carey [2], which was heated on one side only. Because partially-heated channels were used in these experiments, the results of this study are most directly applicable to vaporization in channels heated only on one side. Forced-convective boiling for such circumstances can occur, for example, in evaporator cold plates for electronics cooling applications, as described in ref. [5]. One-sided heating of the evap-

orator passages results from mounting of electrical components so that they contact one side of the cold plate.

Other high-heat-flux thermal control applications in which one-sided heating of an evaporator passage can potentially occur include cooling of fusion reactor walls, cooling of mirrors for high-power lasers, and central receiver heat removal for concentrating solar collector systems. Because of their potential applicability to these systems, the results of this investigation have an intrinsic value of their own.

In general, flow boiling in partially-heated cross-ribbed channels may be expected to differ somewhat from flow boiling in a fully-heated channel with the same geometry. However, comparisons of the results of Xu and Carey [2] and those of the present study with results obtained for fully-heated cross-ribbed channels suggest that many features of the two-phase transport in partially- and fully-heated channels are the same. Specifically, the results obtained by Panchal *et al.* [1], Marseille *et al.* [4] and Ohara and Takahashi [3] for flow boiling in fully-heated channels indicate that the sequence of flow regimes (bubbly to slug to annular to dispersed flow) and the sequence of heat transfer mechanisms (nucleate boiling dominated to film evaporation dominated to liquid-deficient film vaporization) with increasing quality, apparently are the same as those observed in the present study and in the study of Xu and Carey [2] for partially-heated channels. Trends in measured flow boiling heat transfer coefficients for partially- and fully-heated cross-ribbed channels are also very similar. These similarities suggest that the presence of the thermally inactive wall alters the flow and heat transfer from the heated portion of the channel only slightly from that observed in fully-heated channels.

Although the effects of geometry differences are determined in the present study specifically for partially-heated channels, the above observations imply that the effects of the same geometry changes on the flow-boiling transport in fully-heated channels should be similar in many respects. Consequently, the fundamental understanding of the interaction between the channel geometry and the two-phase transport mechanisms obtained in this study for partially-heated cross-ribbed channels also serves to illuminate possible effects of geometry variations, and their causes, for flow boiling in fully-heated cross-ribbed channels. Hence, the results of this investigation are also valuable for the insight they provide regarding flow boiling in fully-heated channels of this type.

Experimental data are reported here for upward flow boiling of R-113 and methanol with the channel oriented vertically for wide ranges of mass flux and quality. The data for the three different cross-ribbed geometries are compared to assess the effects of varying the rib-crossing pattern and rib angle on heat transfer. The results are also compared with those obtained by Xu and Carey [2] to assess the effect of changing rib spacing on heat transfer performance.

EXPERIMENTAL APPARATUS

The experimental studies summarized here were conducted using a test section like that shown in Fig. 1. One end of the rectangular copper slab shown in this figure was machined to form parallel ribs oriented at an angle θ of either 30° or 60° to the flow direction. These ribs have a rectangular cross section, which is an idealization of the more rounded ribs usually found in ribbed-plate heat exchangers. The rib dimensions t, L and H were 1.6, 28.6 and 3.2 mm, respectively. Ribs with the same dimensions and spacing were also machined into a polycarbonate (Lexan) sheet. This insert and the copper slab fit into the assembly shown in Fig. 1 to form a channel with cross-ribbed walls.

The side walls of the channel are Teflon to minimize lateral heat loss, and the inner transparent polycarbonate cover plate on top of the insert forms the top wall of the channel to allow visual observation of the boiling process all along the test section. A second transparent polycarbonate sheet covers the inner one, as shown in Fig. 1, to reduce heat losses from the top of the assembly. The channel thus formed is 1.91 cm wide, 6.4 mm deep and 45.7 cm long. The hydraulic diameter based on the heated perimeter d_{hp} and the hydraulic diameter based on the wetted perimeter d_h for each geometry in this study are listed in Table 1.

The copper slab was heated at the bottom end by two electrical resistance heaters, which provided a virtually uniform heat input along the length of the channel. Heat is conducted from the heaters along the copper slab to the finned surface where it is transferred to the fluid in the channel. The back of the copper slab and heater assembly was completely enclosed in insulation so that heat leakage to the surroundings was negligible.

Thermocouples were embedded in the copper slab, as indicated in Fig. 1, to determine the temperature gradient and surface temperature at four locations along the length of the channel. The first through fourth thermocouple locations were at 7.6, 17.8, 27.9 and 38.1 cm downstream of the inlet, respectively. Small diameter thermocouples (0.9 mm beads) were used to measure the temperature distribution in the copper. These thermocouples were installed in precisely located 1 mm diameter holes drilled to the center line of the copper slab. The spacing between the first and third thermocouples was sufficiently large (19 mm) that uncertainty in the bead locations was small compared to the separation distance. For the boiling data, the temperature difference between the first and third thermocouples was typically greater than 4°C. A least-squares fit of a straight line to the three thermocouple readings was used to determine the temperature gradient and surface temperature. Generally, all three points fit the line very closely. The measured temperature gradient was used to calculate the heat flux to the surface.

Thermocouples were also installed through the channel wall at these locations to measure the local

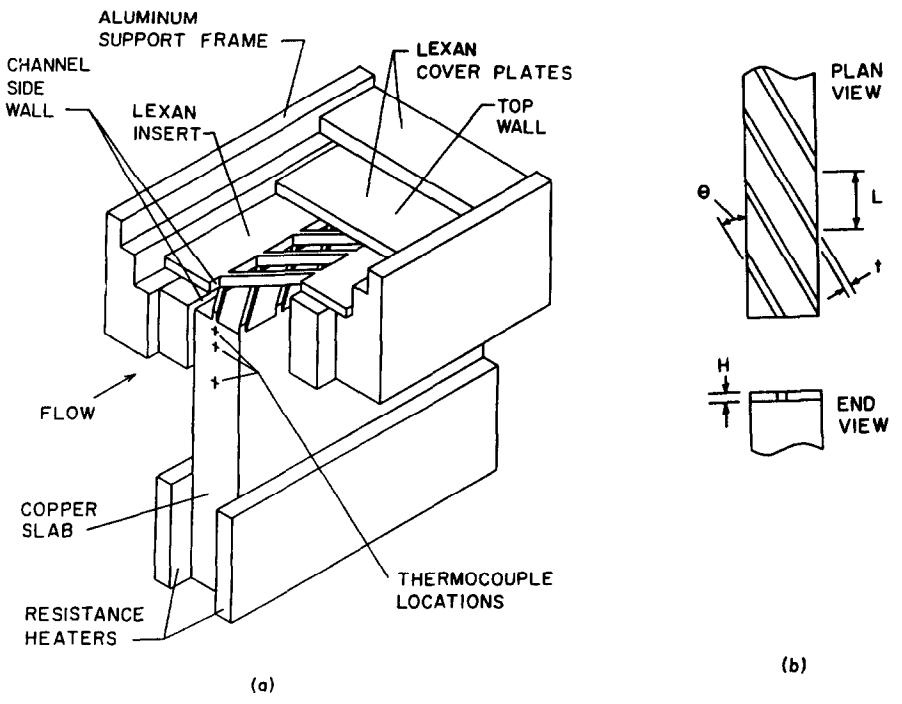

FIG. 1. (a) Cutaway view of test section. (b) Rib geometry variables.

fluid temperature. This result was combined with the calculated heat flux and surface temperature to compute the local heat transfer coefficient. The thermocouple wires and bead inserted into the flow were small compared with the channel dimensions and visual observations indicated that the flow was not significantly affected by them. Thermocouples in the test section were read using an Omega two-pole selector switch and a precision Fluke digital readout with a resolution of ± 0.06°C. With this configuration, the uncertainty in the heat flux is estimated to be $\pm 6\%$ and the uncertainty in the heat transfer coefficients is estimated to be $\pm 11\%$.

A small pump was used to deliver a steady flow of liquid from a reservoir to the test section. The flow leaving the test section went to a water-cooled condenser. Liquid coolant leaving the condenser was returned to the reservoir. The power to heaters in the reservoir, and the condenser water flow rate could be varied to control the temperature of the liquid at the inlet to the test section. The flow rate to the test section was set using a flow control valve.

The liquid flow rate to the test section was measured using a Cole Parmer rotameter. This flow meter was calibrated at several liquid temperatures so that the effect of property variation with temperature was taken into account. Separate rotameter calibration curves were determined for water, R-113 and methanol. The pressure at the exit of the test section was measured with a calibrated gauge. Local pressures along the channel were not directly measured, but they could be inferred from measurements of the local saturation temperature downstream of the onset of saturated boiling.

Table 1. Dimensions of geometry variables

Geometry	θ	L (mm)	H (mm)	t (mm)	d_h (mm)	d_{hp} (mm)
1	30°	28.6	3.2	1.6	6.78	16.5
2	30°	28.6	3.2	1.6	6.78	16.5
3	60°	17.1	3.2	1.6	6.83	16.7
4	30°	17.1	3.2	1.6	5.20	12.1

Prior to running the heat transfer experiments, the ribbed surface of the copper slab was cleaned with a mild acid solution and then thoroughly rinsed before filling the system with the test liquid. The Lexan cover plate and ribs were also rinsed as part of this pretest cleaning process. This procedure kept the finned copper surface clean and free of tarnish throughout the test program. It also helped maintain consistency in the nucleation characteristics of the surface.

In the experiments reported here, the channel was positioned vertically with upward flow. Power to the heaters in the test section was controlled by two rheostats which could be adjusted to vary the heat input to the channel. The three different rib-crossing patterns tested in these experiments are shown schematically as surfaces 1, 2 and 3 in Fig. 2. A schematic representation of the rib crossing pattern for the surface tested by Xu and Carey [2] is also shown as surface 4 in Fig. 2. For surface 4, H, t and θ were identical to those for surfaces 1 and 2, but L for surface 4 was smaller, being only 17.1 mm.

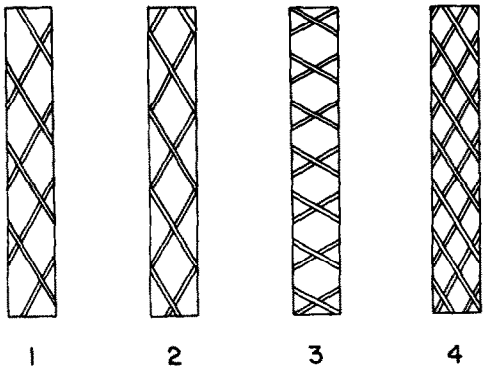

FIG. 2. Schematic of the four rib geometries. The front-surface ribs for geometries 1 and 2 are 180° out of phase. Surface 4 is the surface tested in Xu and Carey [2].

EXPERIMENTAL PROCEDURE

Prior to running the convective boiling experiments, the single-phase heat transfer characteristics were determined experimentally for each of the ribbed channel configurations 1, 2 and 3 shown in Fig. 2. Local heat transfer coefficients were measured at low heat flux and high inlet subcooling where no vaporization occurs. After setting the flow rate and power to the heaters at the desired levels, the system was allowed to stabilize for 10–15 min before thermocouple and flow readings were taken. The resulting single-phase heat transfer data for water are plotted in non-dimensional form in Fig. 3. The measured heat transfer coefficients represented in Fig. 3 are average values over the heated perimeter of the channel at each downstream location where thermocouple measurements were made. These values of h were iteratively calculated from the following energy balance relation:

$$W_c L_c k_c \nabla T_c = h(A_P + \eta_R A_R)(T_W - T_M) \quad (1)$$

where ∇T_c is the measured local temperature gradient in the copper and η_R the fin efficiency of the ribs given by

$$\eta_R = \frac{1}{M(H+t/2)}\left[\frac{\tanh(MH)+h/k_c M}{1+(h/k_c M)\tanh(MH)}\right]$$

$$M = \sqrt{(2h/k_c t)}. \quad (2)$$

In the flow boiling experiments, the system was allowed to stabilize at the selected power and flow settings before data were taken. The thermocouple readings and the liquid flow rates were recorded in the same manner as for the single-phase data. The test fluid entered the channel as subcooled liquid. The downstream location where saturated nucleate boiling first began was determined by visually inspecting the flow in the channel. This zero quality point was typically 20–30 hydraulic diameters downstream of the inlet. Boiling heat transfer data were obtained at the three thermocouple locations nearest the exit end which were 34, 54 and 73 hydraulic diameters downstream of the inlet.

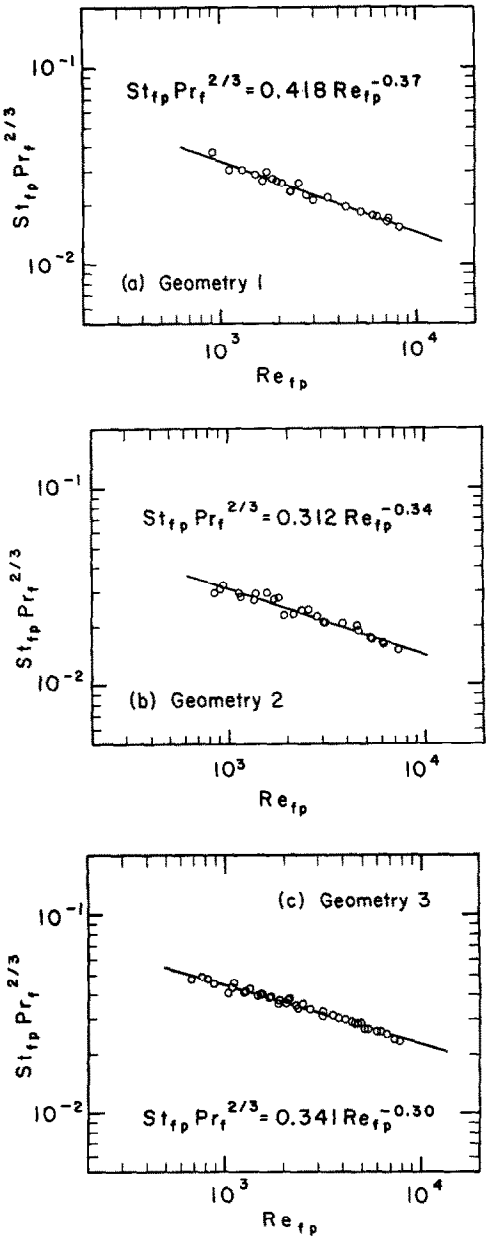

FIG. 3. Single-phase heat transfer data for surfaces 1, 2 and 3.

As for single-phase flow, the local heat transfer coefficient was obtained by iteratively solving equations (1) and (2) using the measured data at the location of interest. However, in the saturated boiling experiments, T_M in equation (1) was equal to T_{SAT}, the saturation temperature of the coolant. The local boiling heat transfer coefficients calculated in this manner are average values over the heated perimeter of the channel. Fin efficiencies for the boiling data points were typically near 90% for the conditions tested here.

The mass flux, G, was determined from the flow meter reading and the geometry of the channel. The banks of thermocouples embedded in the copper slab provided the local variation of the surface heat flux along the entire heated length of the channel. This information was combined with the measured mass flow rate in an energy balance to compute the local quality at each thermocouple station downstream of the onset of saturated boiling.

As noted above, the downstream location where saturated nucleate boiling began was determined by visually inspecting the flow. This zero quality point was taken to be the lowest vertical location where continuous growth and release of vapor bubbles occurred and vapor bubbles were present throughout the liquid flow in the channel. An energy balance on the fluid from the test section inlet to the two-phase zone yielded essentially the same location for the point of zero quality. The quality x at the three uppermost thermocouple locations was therefore determined from an energy balance over the portion of the channel downstream of the visually-determined location of $x = 0$. Calculations using the measured data thus indicated the value of h_{tp} which corresponded to specific values of x and G.

Values of h_{tp} were determined for convective boiling of R-113 and methanol for values of quality and mass flux in the ranges $0.10 < x < 0.8$ and $40 < G < 230$ kg m^{-2} s^{-1}. Mass flux levels between 40 and 230 kg m^{-2} s^{-1} are commonly encountered in evaporators for small refrigeration and air-conditioning systems and other thermal control applications in which a low evaporator pressure drop is desirable. Specific examples include automotive air-conditioning evaporators, and evaporator cold plates for electronics cooling (see ref. [5]). Hence, the results of these experiments relate most directly to applications of this type. Values of heat flux up to 300 kW m^{-2} were used in these experiments. The estimated uncertainty in the measurements is $\pm 5\%$ for G, $\pm 9\%$ for x and $\pm 11\%$ for h_{tp}. The reproducibility of the heat transfer data was checked and found in all cases to be better than the uncertainty in the measurements.

RESULTS AND DISCUSSION

The single-phase heat transfer data for the three cross-ribbed configurations tested in this study are shown in non-dimensional form in Fig. 3. The optimal curve fits to the data for each of these surfaces are shown together in Fig. 4. Also shown in Fig. 4 is the curve fit to the single-phase data obtained by Xu and Carey [2] for geometry 4 in Fig. 2. It can be seen that in terms of the Colburn j-factor ($St_{fp} Pr_f^{2/3}$) vs Reynolds number representation, there is very little difference in the performance of surfaces 1 and 2. Optimal curve fits to the data for each surface are slightly different, with that for surface 1 being slightly higher for the range of Reynolds numbers tested. This suggests that variation of the rib-crossing locations, relative to the sidewalls, has little, if any effect, on single-phase heat transfer.

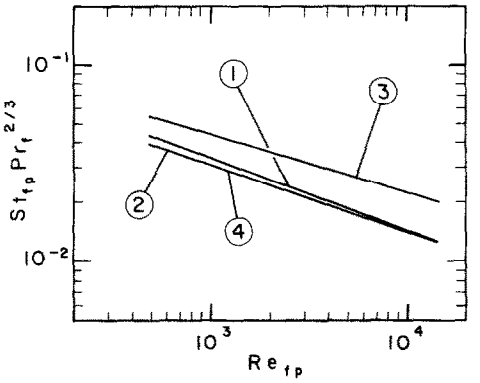

FIG. 4. Comparison of single-phase heat transfer curves for geometries 1–4.

It can also be seen that the single-phase heat transfer data for these surfaces agrees almost exactly with the curve fit to data obtained by Xu and Carey [2] for surface 4. The only difference between these surfaces is that for surface 4 the ribs are spaced more closely together. This suggests that moderate variation of the rib spacing does not strongly affect the single-phase heat transfer performance of these surfaces.

On the other hand, geometry 3 with ribs at an angle of 60° to the flow direction is seen in Fig. 4 to have a significantly higher j vs Reynolds number curve than the other geometries having 30° ribs. This would seem to suggest that greater mixing and enhancement in single-phase flow is obtained when the rib axis is more oblique to the flow direction.

For all the convective boiling experiments summarized here, the flow in the test section was vertically upward. During these experiments, the flow was invariably in the bubbly regime near the location of the onset of saturated boiling. However, a very short distance downstream of this location, the flow typically had undergone a transition through slug flow and into churn or annular flow. Consequently, the two-phase flow was in an annular film flow regime (either churn or annular flow) over almost the entire vaporization process in the channel. These characteristics of the boiling process were observed for both coolants tested.

Photographs of the two-phase flow in the test section for geometries 1 and 3 in Fig. 2 are shown in Fig. 5. In Figs. 5(a) and (c), an annular flow at moderate quality levels is shown. For these conditions, a relatively thick liquid film covers the entire surface of the channel wall. Figures 5(b) and (d) show the flows observed somewhat further downstream and/or at higher quality where the liquid inventory has further diminished. At these locations portions of the back (copper) wall of the channel have become dry and appear as light patches against the darker wetted surface of the rest of the channel wall.

For all the channel geometries tested, photographs,

video recordings and visual observations of the flow all indicate that the ribs induce a swirling effect on the liquid film along the wall during annular flow. Although there is some tendency for the film to wash over the ribs, for the most part the liquid film follows the ribs diagonally across the channel. When the film reaches and collides with one of the lateral walls, liquid in the film is transferred to the opposite ribbed wall, whereupon it moves diagonally back across the channel in the opposite direction.

Because the front ribbed surface of the test section is adiabatic, and liquid which begins to move across it (from right to left in Fig. 5) will eventually reach the opposite lateral wall and be returned to the copper surface on the left-hand side of the test section. However, because the liquid film on the copper (back) wall of the channel is evaporating, at high qualities, portions of the film moving across it (from right to left in Fig. 5) may evaporate almost completely. As a result, dryout was usually observed first along the right edge of the channel as the flow proceeded downstream, even though the left-hand side of the copper surface in the channel was well supplied by liquid flowing there downstream over the ribs and along the ribs on the adiabatic surface.

It is difficult to clearly see in Figs. 5(b) and (d) whether the left- or right-hand side of the copper (back) surface is drier. However, it can be seen in these figures that the left-hand side of the adiabatic (front) wall of the channels in Figs. 5(b) and (d) is covered with more liquid than the right-hand side. Because the right-hand side of the copper (back) surface is very dry, it feeds very little liquid onto the adiabatic wall. Consequently, little liquid flows diagonally across the front wall to the left-hand side of the channel. On the left-hand side, flow of liquid directly downstream over the ribs on the adiabatic front wall keeps the surface well-wetted with liquid, maintaining some flow of liquid onto the heated copper surface. Because liquid is being supplied to the heated back wall at this

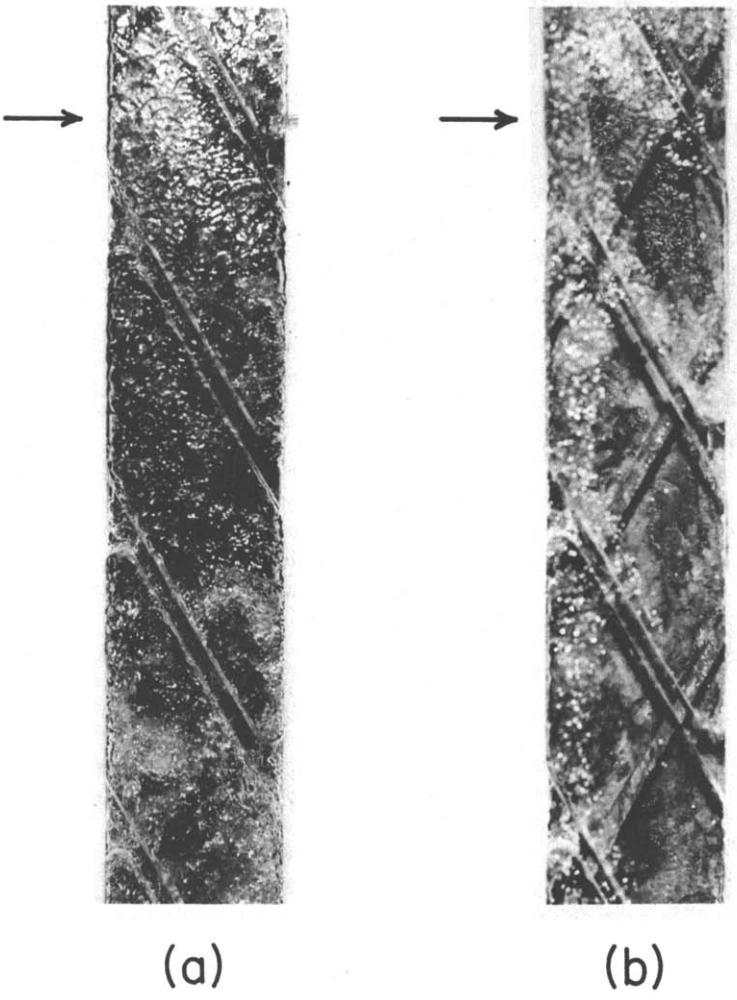

FIG. 5. Photographs of annular film-flow evaporation in cross-ribbed channel geometries 1 ((a) and (b)) and 3 ((c) and (d)). In photographs (a) and (c), the walls are fully wetted, whereas portions of the wall (light areas) are dry in (b) and (d). All photographs are for $G = 111$ kg m^{-2} s^{-1}. At the thermocouple locations denoted by the arrows, the quality is equal to (a) 0.34, (b) 0.65, (c) 0.19 and (d) 0.31.

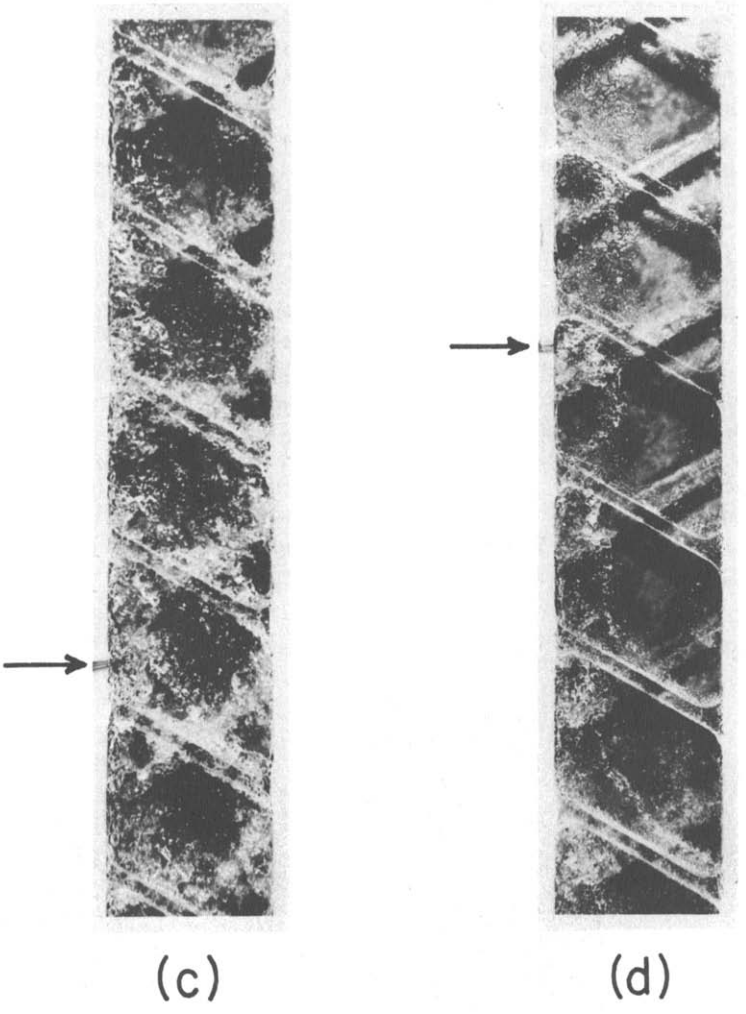

FIG. 5.—*Continued.*

location, the left-hand side of the heated surface generally tends to stay wetted to a greater degree than the right-hand side, once the surface begins to dry out. In Figs. 5(a) and (c) it visually appears that for comparable conditions, there is more liquid being dragged directly over the ribs in the downstream direction for geometry 3 with the 60° ribs than there is in geometry 1 with 30° ribs.

The exchange of liquid between the front and back walls of the channel, facilitated by the lateral walls, apparently plays an important role in the transport for annular two-phase flow in channels of this type. Since some liquid is swept directly downstream over the ribs, it would appear that the amount of liquid transferred between the walls in this manner would be very small if the lateral width of the channel was very large. For annular flow, liquid initially on the front wall would then be more likely to stay on the front wall, and liquid initially on the back wall would tend to stay on the back wall. Transfer of liquid between the front and back walls would be largely due to entrainment and deposition for such circumstances. However, for the relatively small lateral channel widths typically encountered in compact evaporators for air-conditioning applications (2–10 cm [3, 4]), the results of our investigation suggest that the lateral walls will provide an important means of transferring liquid between the front and back (or top and bottom) walls.

The vertical flow conditions at which data were obtained for geometry 3 are shown on a flow regime map of the type proposed by Hewitt and Roberts [6] in Fig. 6. The approximate location of the churn to annular flow regime transition indicated by our observations is shown as a broken line in Fig. 6. Similar maps have been constructed for the other geometries tested in this study. The churn to annular flow regime transitions observed for all these geometries are consistent with the two-phase flow regime observations of Xu and Carey [2] for geometry 4.

As described above, the flow in the test section was generally observed to undergo a transition to annular film flow a short distance downstream of the onset of saturated boiling. In virtually all our experiments, it appeared visually that this flow regime transition was accompanied by almost complete suppression of

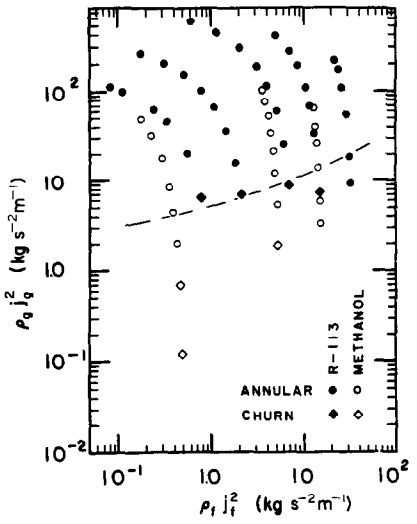

FIG. 6. Visually observed flow regimes for geometry 3. The broken curve denotes the approximate transition between churn and annular flow.

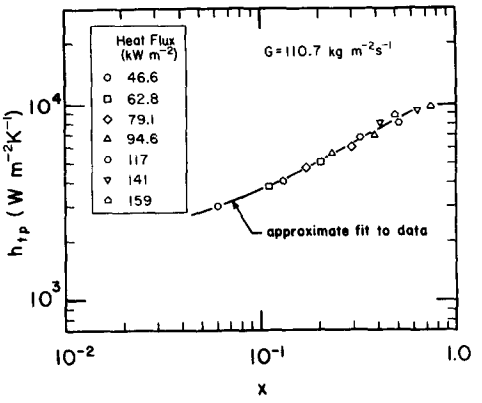

FIG. 8. Convective boiling heat transfer data for geometry 3 at a mass flux of 110.7 kg m^{-2} s^{-1}. The test fluid is R-113.

nucleate boiling on the heated portion of the channel wall. Nucleate boiling could sometimes be observed in corner regions just downstream of the ribs and along the lateral walls. However, for most of the heated surface between the ribs, and the upstream face and top of the ribs, there appeared to be very little, if any, nucleate boiling present.

In spite of our visual observations indicating that very little nucleate boiling was present, our heat transfer coefficient data for geometries 1 and 2 were found to vary significantly with heat flux at low to moderate quality for the higher heat fluxes applied in our experiments. For geometry 1, heat transfer data obtained for R-113 mass fluxes of 41.8 and 111.3 km m^{-2} s^{-1} at several different levels of applied heat flux are shown in Fig. 7.

It can be seen in Fig. 7 that at these fixed mass flux conditions, increasing the heat flux generally increases the heat transfer coefficient. This is exactly the trend expected if nucleate boiling effects contribute significantly to the overall heat transfer. A similar dependence of the measured heat transfer coefficient on heat flux was also observed in the methanol data for geometry 1 and in the methanol and R-113 data for geometry 2. This type of heat flux dependence was observed over the full range of mass flux values covered in our experiments with these two channel geometries. Hence our heat transfer data suggest that for these geometries, nucleate boiling is present to a significant degree in the flow boiling processes examined here.

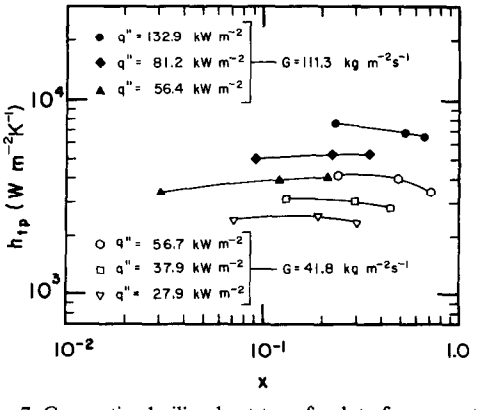

FIG. 7. Convective boiling heat transfer data for geometry 1.

In contrast to the results for geometries 1 and 2, convective boiling heat transfer data for geometry 3 shows virtually no dependence on heat flux, except for a few data points obtained very near the location where the onset of boiling occurred. Heat transfer data obtained for an R-113 mass flux of 110.7 kg m^{-2} s^{-1} at several heat flux levels are shown in Fig. 8. It can be seen in this figure that all the data essentially fall on a single curve, in spite of the variation in the heat flux among these data. This trend was, in fact, observed over the full range of mass flux values tested and for methanol as well as R-113. As noted previously, the heat transfer data obtained by Xu and Carey [2] for geometry 4 also showed no significant dependence on heat flux.

The difference in the effect of heat flux on the heat transfer data between surface 3 and surfaces 1 and 2 is believed to be due to the manner in which the ribs affect suppression of nucleation for each geometry. Surfaces 3 and 4 in Fig. 2 both strongly agitate the flow. In the case of geometry 3, the strong agitation results from the more oblique angle of the ribs to the flow direction and the washing of liquid over the ribs in the downstream direction. In the case of geometry 4, the strong agitation apparently is the result of the tighter spacing of the ribs and the higher frequency of the rib crossing locations which causes the vapor to twist and turn more frequently as it flows through the channel. In geometries 1 and 2, the rib angle is smaller than that for geometry 3 and the distance between ribs is larger. As a result, a larger fraction of the channel wall consists of long stretches of uninter-

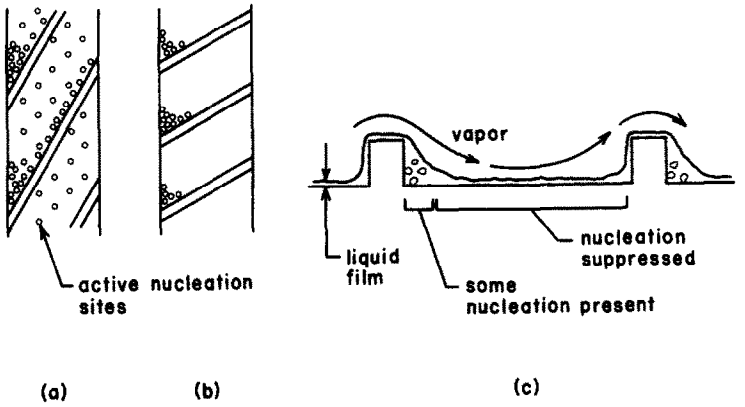

FIG. 9. Postulated occurrence of nucleate boiling based on visual observations and heat transfer data: (a) geometry 2—front view; (b) surface 3—front view; (c) surface 3—side view.

rupted film flow. The convective evaporation effect is expected to be less enhanced for these circumstances relative to geometries 3 and 4 which agitate the liquid film flow more strongly.

The stronger enhancement of the forced convective evaporation effect due to increased agitation in geometries 3 and 4 would tend to more strongly suppress nucleation. Some nucleation on the leeward side of the ribs, as shown schematically in Fig. 9(c), is still expected because of the tendency for the liquid film to be thicker there. Nucleation at such locations was in fact observed visually in our experiments, as noted above. For geometries 1 and 2, we also visually observed nucleation just downstream of the ribs for the same reason. Our heat transfer data suggest that some scattered nucleation activity was also present between the ribs, as indicated in Fig. 9(a), although we had difficulty visually detecting such sites. The increased suppression with increasing enhancement of the film evaporation process suggested by these trends is consistent with the absence of nucleation activity reported by Xu and Carey [2] for geometry 4 under conditions at which correlations for a simple round tube indicate that substantial nucleate boiling effects are present.

Because the data for geometry 3 were essentially independent of heat flux, for a given coolant and system pressure, the heat transfer coefficient can be considered to be a function of mass flux and quality. The experimentally-determined variations of the convective boiling heat transfer coefficient with G and x for R-113 and methanol are shown in Fig. 10. For moderate to high quality, the general trend of increasing heat transfer coefficient with quality and mass flux seen in Figs. 10(a) and (b) is consistent with the results obtained by Xu and Carey [2] for geometry 4.

It can be seen in Fig. 10 that at high qualities ($x > 0.75$), the heat transfer coefficients generally decrease as the quality increases. This occurs because the liquid film dries out over portions of the heated surface for qualities above about 0.75. Dry portions of the surface do not participate in the vaporization process, reducing the overall mean heat transfer coefficient at that downstream location. The surface becomes progressively drier with increasing downstream distance, and the heat transfer coefficient drops towards the value for pure vapor flow alone. A similar decrease in h_{tp} with increasing x at high quality was observed by Xu and Carey [2] and Ohara and Takahashi [3] for flow boiling in the cross-ribbed geometries considered in their investigations.

To assess the enhancement characteristics of each

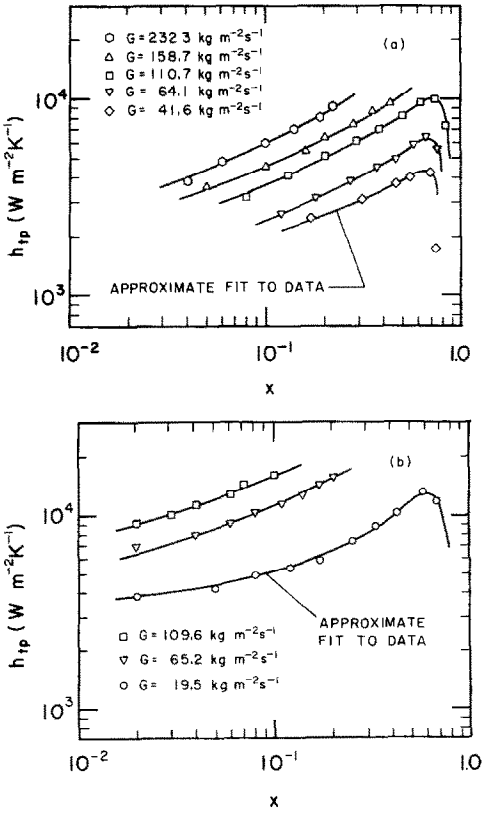

FIG. 10. Convective boiling heat transfer data for geometry 3 using (a) R-113 and (b) methanol as test fluids.

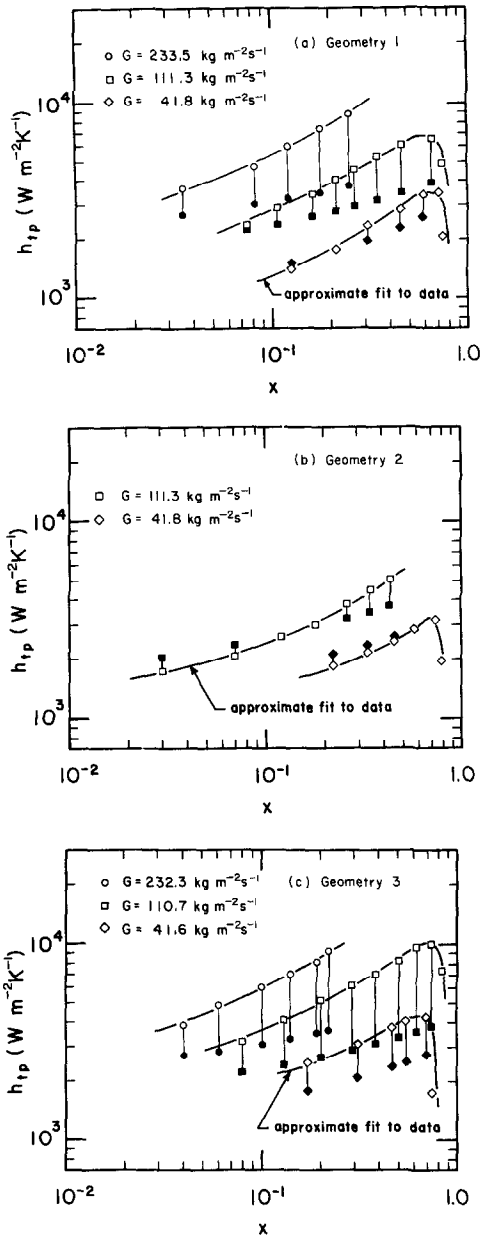

FIG. 11. Comparison of convective boiling heat transfer data for geometries 1–3 (open symbols) with heat transfer coefficients predicted by the Bennett and Chen [7] correlation (solid symbols) at the same wall superheat and flow conditions. For all data shown the test fluid is R-113.

of the cross-ribbed geometries considered here, representative convective boiling heat transfer data for geometries 1, 2 and 3 are plotted in Fig. 11 together with the corresponding heat transfer coefficient predicted by the Bennet and Chen [7] correlation for round tubes under comparable conditions. Specifically, h_{tp} values were computed at the mass flux, quality, wall superheat and the hydraulic geometry d_h corresponding to each cross-ribbed data point shown in these plots. Since the Bennett and Chen correlation [7] is not appropriate at qualities beyond the onset of dryout, round tube values were not computed for points clearly in the partial dryout range.

The cross-ribbed data shown in these plots for geometries 1 and 2 were obtained at the thermocouple location furthest downstream (nearest the exit). For a constant flow rate, the heat flux was varied to achieve the range of qualities shown in these plots. Because the heat transfer coefficient varies somewhat with heat flux for these two geometries, the h_{tp} vs x curves for the given G values in Figs. 11(a) and (b) correspond to a specific variation of heat flux along the channel. Since the heat transfer data for geometry 3 show virtually no heat flux dependency, the variation of h_{tp} with x for the given G values is expected to represent the performance of the surface for any heat flux in the range tested here ($q'' \leqslant 300$ kW m^{-2}).

It can be seen in Fig. 11 that for given G and x values, the heat transfer coefficient for geometries 1 and 3 are generally significantly higher than the corresponding values predicted by the round tube correlation. On the other hand, the measured values of h_{tp} for geometry 2 are relatively close to the corresponding round tube values. Because the ribs are widely spaced and there are few rib-crossing locations to agitate the flow, it would not be surprising if the convective boiling heat transfer performance of geometry 2 was not too different from that for an ordinary rectangular passage.

It should be noted that using the channel hydraulic diameter as an effective tube diameter in the Bennett and Chen [7] correlation may not yield a prediction of h_{tp} which agrees perfectly with data for a rectangular passage because the round tube correlation does not account for variations of the convective effect and the nucleate boiling contribution in the corner regions. Thus, the data points computed using the Bennett and Chen [7] correlation in Fig. 11 are not expected to exactly agree with the performance of a plain rectangular passage with the same hydraulic diameter. However, since the corner regions are only a small portion of the overall perimeter of the channel, h_{tp} values predicted in this manner should be close to the actual values for a rectangular channel.

It can be seen, in fact, that the measured h_{tp} data for geometry 2 are close to the predictions of the Bennett and Chen [7] correlation, being somewhat below them at low quality, and somewhat above them at higher quality. The amount by which the data are below the correlation predictions is small, and could be due to differences between the surface nucleation characteristics implicitly built into the correlation and those that actually existed during our flow boiling experiments in geometry 2 at low quality. At higher quality, where the mean flow velocity (for a given G value) is much higher, the ribs apparently do provide some enhancement, resulting in h_{tp} values somewhat higher than those predicted by the round tube correlation. It is also possible, however, that some of the deviation in the high and low quality ranges may just be a consequence of differences between the round

tube predictions and the actual convective boiling performance for rectangular channels, as discussed above.

The significantly higher measured h_{tp} values for geometry 1, relative to geometry 2 at the same conditions apparently is due to the increased number of rib-crossing locations, since all other features are identical. This seems to imply that the increased number of crossing locations results in increased agitation of the flow, which, in turn, enhances the flow boiling heat transfer.

The enhancement of geometry 3 relative to the round tube is clearly the greatest of the three cross-ribbed configurations tested here. The convective boiling heat transfer coefficients for this geometry are as much as a factor of three above corresponding values predicted for a round tube for comparable conditions. This level of enhancement is comparable to that observed by Xu and Carey [2] for geometry 4.

For geometries 1 and 2, the dependence of the heat transfer coefficient on heat flux suggests that correlation of the convective boiling heat transfer data must account for both nucleate boiling and convective evaporation effects. Further study of nucleate boiling effects during flow boiling in these geometries is needed to fully resolve the nature of the interaction between these mechanisms. However, for geometry 3, the apparent lack of nucleate boiling effects suggests that annular film-flow evaporation is the dominant vaporization over most of the quality range of interest in applications.

To correlate the data for this channel configuration, the use of parameters developed for round tubes and other geometries might, at first glance, seem inappropriate because of the geometry differences. However, for annular film flow, the liquid film is often very thin, and large-scale variations of the channel wall geometry may have only a secondary effect on local transport. This supports the contention that correlation techniques developed for annular film-flow evaporation in round tubes and other geometries may be adapted to the more complex geometries considered here. Xu and Carey [2] did, in fact, find that the annular film-flow boiling data for geometry 4 were well correlated in terms of dimensionless parameters used by Carey *et al.* [5] to correlate similar data for a channel with offset strip fins.

In this study we evaluated two correlation schemes as possible methods for correlating the annular film-flow boiling data for geometry 3. Both of these methods were originally developed for other types of geometries. The specific methods considered were (1) the correlation scheme proposed by Carey and Mandrusiak [8] which is based on an approximate integral model analysis of transport in the liquid film, and (2) the F vs Martinelli parameter correlation proposed by Bennett and Chen [7] for prediction of the forced-convective evaporation contribution to the overall convective boiling heat transfer coefficient in round tubes.

The approximate annular flow model developed by Carey and Mandrusiak [8] implies that the heat transfer data for annular film-flow boiling in a partially-heated channel can be correlated in terms of a parameter Ψ and the Martinelli parameter X_{tt} defined as

$$\Psi = \frac{h_c}{h_{fp}} \frac{4.74\sqrt{A}\tan^{-1}(0.149\sqrt{(Re_{fp}\,Pr_f)}\sqrt{(d_h/d_{hp})})}{Re_{fp}^{n/2}\,Pr_f^{1/6}(d_{hp}/d_h)^{n/2}} \tag{3}$$

$$X_{tt} = \left[\frac{(dp/dz)_{Ff}}{(dp/dz)_{Fg}}\right]_{tt}^{1/2}. \tag{4}$$

In the above definition of Ψ, h_c is the convective boiling heat transfer coefficient in the absence of nucleate boiling effects, and h_{fp} the single-phase heat transfer coefficient for the liquid phase flowing alone in the channel. The variables d_{hp} and d_h are hydraulic diameters based on heated and wetted perimeters, respectively.

In the Martinelli parameter given by equation (4), the single-phase pressure gradients are evaluated as

$$(dp/dz)_{Ff} = -\frac{2f_f G^2(1-x)^2}{\rho_f d_h} \tag{5a}$$

$$(dp/dz)_{Fg} = -\frac{2f_g G^2 x^2}{\rho_g d_h}. \tag{5b}$$

The single-phase friction factors in equations (5a) and (5b) are calculated using the modified Reynolds analogy together with the experimentally determined heat transfer correlation, as proposed by Carey and Mandrusiak [8]

$$f_f/2 = St_f\,Pr_f^{2/3} = A\,Re_f^{-n} \tag{6a}$$

$$f_g/2 = St_g\,Pr_g^{2/3} = A\,Re_g^{-n}. \tag{6b}$$

Combining equations (4)–(6), the relation for the Martinelli parameter becomes

$$X_{tt} = \left(\frac{\rho_g}{\rho_f}\right)^{1/2}\left(\frac{\mu_f}{\mu_g}\right)^{n/2}\left(\frac{1-x}{x}\right)^{1-n/2}. \tag{7}$$

In Fig. 12, heat transfer data obtained for geometry 3 are plotted in terms of X_{tt} and Ψ. Figures 12(a) and (b) show data for R-113 and methanol, respectively. The open symbols in these plots denote data points for which the flow was observed to be in the annular flow regime. The solid symbols similarly denote data in the churn flow regime. The single partially-filled symbol in Fig. 12(a) denotes a data point for which the surface was observed to be partially dry. This point is below the trend in the other non-dryout data because of the reduction in the heat transfer coefficient associated with partial dryout of the heated surface.

In general, it can be seen that for both fluids tested, the data obtained over wide ranges of quality and mass flux correlate well in terms of Ψ and X_{tt}. The data for churn flow are also consistent with the annular flow trend. As indicated in Figs. 12(a) and

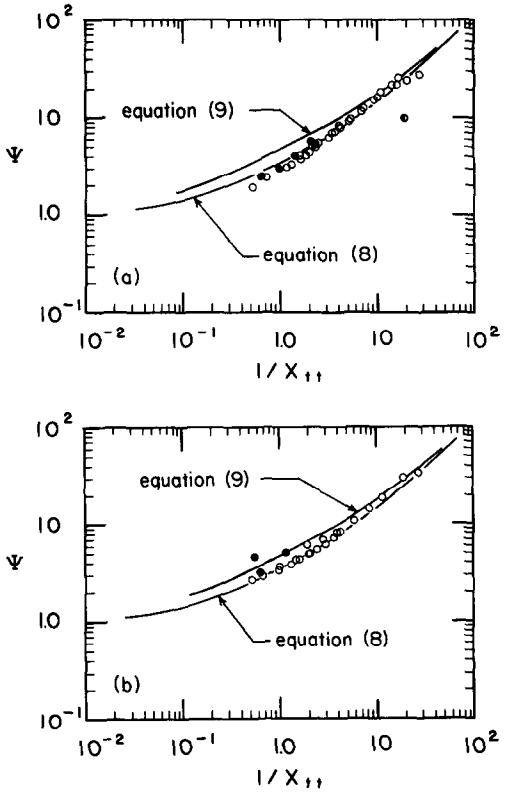

FIG. 12. Comparison of the measured heat transfer data for convective boiling in geometry 3 with the correlation proposed by Carey and Mandrusiak [8]. Data shown are for (a) R-113 and (b) methanol. The solid symbols and open symbols denote churn and annular flow, respectively.

(b), a best fit to the data for this geometry is provided by the relation

$$\Psi = \left[1 + \frac{10}{X_{tt}} + \frac{1.0}{X_{tt}^2}\right]^{1/2}. \quad (8)$$

Also shown in Figs. 12(a) and (b) is the following relation between Ψ and X_{tt} obtained from theoretical arguments for a simple rectangular channel (without ribs or fins) or a round channel by Carey and Mandrusiak [8]

$$\Psi = \left[1 + \frac{20}{X_{tt}} + \frac{1}{X_{tt}^2}\right]^{1/2}. \quad (9)$$

The data for geometry 3 are significantly lower than the corresponding Ψ values predicted by equation (9) at lower values of $1/X_{tt}$. At higher values of this parameter, the data differ only slightly from the predictions of this semitheoretical relation. In contrast, Xu and Carey [2] found that Ψ vs X_{tt} data for geometry 4 were consistently about 20% higher than the Ψ values predicted by equation (9) for the same value of X_{tt}. As noted by Xu and Carey [2], there is no a priori reason to believe that equation (9) should fit the data for these geometries. It is noteworthy, however, that the data for these two geometries are close to this theoretically-based relation.

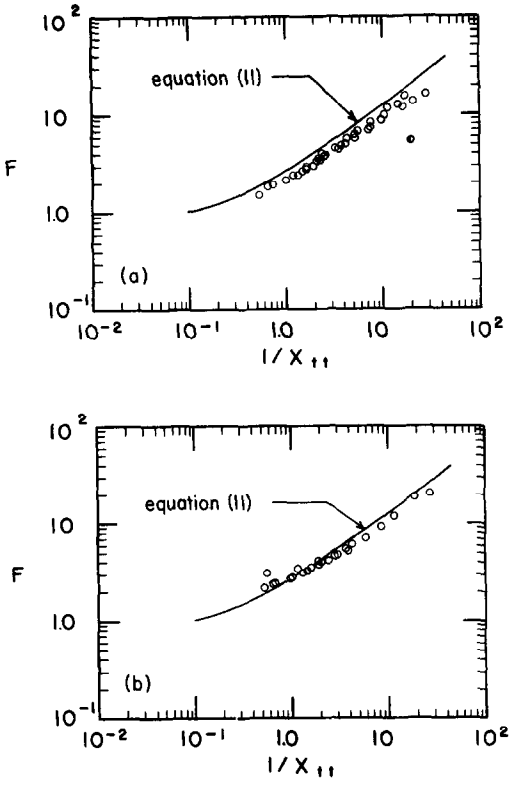

FIG. 13. Comparison of the measured heat transfer data for convective boiling in geometry 3 with the correlation proposed by Bennett and Chen [7]. Data shown are for (a) R-113 and (b) methanol.

For round tubes, the correlating parameters used by Bennett and Chen [7] to predict the forced-convective evaporation contribution to the overall convective boiling heat transfer coefficient were the Martinelli parameter defined by equation (4) and the parameter F defined as

$$F = (h_c/h_{fp})Pr_f^{-0.296}. \quad (10)$$

The data for geometry 3 are plotted in terms of X_{tt} and F in Figs. 13(a) and (b). Equation (7), which is based on the modified Reynolds analogy, was again used to determine the X_{tt} values for the data shown in these figures. Figure 14 also shows the vertical flow

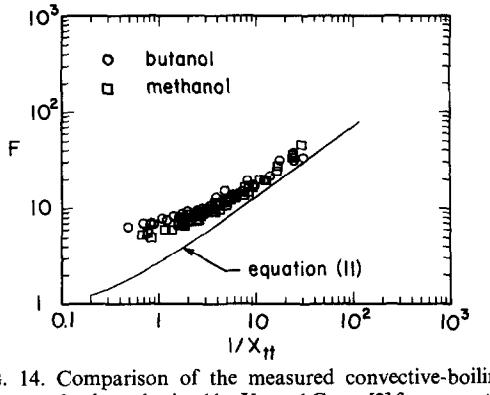

FIG. 14. Comparison of the measured convective-boiling heat transfer data obtained by Xu and Carey [2] for geometry 4 with the correlation proposed by Bennett and Chen [7].

data obtained by Xu and Carey [2] for geometry 4 plotted in terms of X_{tt} and F. This figure shows the same data that are plotted in terms of X_{tt} and Ψ in Fig. 7 of ref. [2]. The plots shown in Figs. 13 and 14 also show the curve representing the original graphical Chen correlation curve as represented by the following empirical expressions developed by Collier [9]

$$F = 2.53\left[0.213 + \frac{1}{X_{tt}}\right]^{0.736}, \quad X_{tt} > 0.1 \quad (11a)$$

$$F = 1.0, \quad X_{tt} \leqslant 0.1. \quad (11b)$$

It can be seen in Fig. 13 that the data for geometry 3 is close to the Chen round-tube curve, but generally a bit lower. In Fig. 14, the data for geometry 4 is again seen to lie near the Chen curve, but for this geometry the data are consistently somewhat above the curve. For each of these geometries individually, the data for different fluids and widely different values of mass flux and quality are well correlated in terms of X_{tt} and F.

CONCLUDING REMARKS

It is clear that the possible combinations of rib angle, rib dimensions and rib spacing that can be used in cross-ribbed channels is virtually limitless. Although the four specific geometries considered in this study represent only a limited number of these combinations, the results of this study do provide some insight into the changes in heat transfer performance produced by varying the rib-crossing pattern, spacing and angle with respect to the mean flow direction.

Among the four geometries considered here, geometries 1 and 2 had lower flow boiling heat transfer coefficients than the others for a given set of conditions. This lower performance appears to be a consequence of the wider rib spacing and lower rib angle for these geometries which apparently provide less enhancement. Even for these geometries, however, significant enhancement over the predicted performance for a comparable round tube was obtained at higher mass flow rates and moderate quality levels. At lower mass flow rates and/or lower qualities, the flow boiling heat transfer coefficients for these geometries were only slightly different from those for round tubes under comparable conditions. Significant nucleate boiling effects were present for these geometries, which is also consistent with the expected flow boiling behavior for round tubes.

The experimental data for geometries 1 and 2 also suggest that the nature of the rib-crossing pattern in the channel also may have an impact on heat transfer. The measured flow boiling heat transfer coefficients in geometry 1 overall were generally about 15% higher than for geometry 2 at the same quality, heat flux and mass flux conditions. Apparently, the additional rib-crossing locations away from the lateral channel walls for geometry 1 (see Fig. 2) enhances the convective boiling process somewhat better. It is interesting, however, that a comparable enhancement for geometry 1 over geometry 2 was not observed for single-phase convection.

The convective boiling heat transfer performance of geometries 3 and 4 were clearly superior to that for geometries 1 and 2. For these geometries, the strong enhancement of convective transport also apparently resulted in almost complete suppression of nucleate boiling effects. For the same quality and mass flux, the measured flow boiling heat transfer coefficients for these two geometries were about equal. The results indicate that these geometries achieve convective boiling heat transfer coefficients that are as much as a factor of three higher than corresponding values for a round tube under comparable conditions.

For each geometry individually, the flow boiling data for geometries 3 and 4 were found to be well correlated either in terms of the parameters X_{tt} and Ψ or X_{tt} and F. The results for geometries 3 and 4 further imply that the $\Psi(X_{tt})$ or $F(X_{tt})$ relation which best fits performance data may vary from one geometry to another. This is consistent with the results of a recent study by Mandrusiak and Carey [10] which indicate a similar variation of the optimal $\Psi(X_{tt})$ or $F(X_{tt})$ relation among different offset strip fin geometries.

It should also be noted that although the Ψ and F values for geometry 4 are higher than corresponding values for geometry 3, the single phase j factor curve for geometry 3 is higher than that for geometry 4. Since the convective boiling heat transfer coefficient is about proportional to the $h_f F$ or $h_f \Psi$ product, these opposite trends in the single-phase and two-phase correlation curves tend to compensate for one another. The overall result is that for comparable flow conditions the convective boiling heat transfer coefficients of these two geometries are about the same.

Since the conclusions noted above are based on our results for partially-heated cross-ribbed channels, they are, of course, most directly applicable to channels of this type that are heated only on one side. However, the strong similarities between the results of our partially-heated channel experiments and published results [1, 3, 4] for fully-heated cross-ribbed channels suggest that performance variations associated with geometry changes in fully-heated channels will be similar to those observed in our partially-heated channels. It therefore seems likely that the conclusions described above will also be applicable to flow boiling in most fully-heated cross-ribbed channel configurations.

From the measured data it is clear that cross-ribbed channel geometries offer the potential for significantly enhanced flow boiling heat transfer performance. The results of this study also indicate, however, that the geometry must be carefully chosen to reap the full benefits of using this type of configuration.

Acknowledgements—Support for this research was provided by the National Science Foundation under research grant No. CBT-8451781.

REFERENCES

1. C. B. Panchal, D. L. Willis and A. Thomas, Convective boiling of ammonia and Freon 22 in plate heat exchangers, *Proc. ASME/JSME Thermal Engng Joint Conf.*, Vol. 2, pp. 261–268 (1983).
2. X. Xu and V. P. Carey, Heat transfer and two-phase flow during convective boiling in a partially-heated cross-ribbed channel, *Int. J. Heat Mass Transfer* **30,** 2385–2397 (1987).
3. T. Ohara and T. Takahashi, High performance evaporator development, SAE Paper No. 880047, presented at the 1988 SAE Int. Congress and Exposition, Detroit, Michigan (1988).
4. T. J. Marseille, V. P. Carey and S. L. Estergreen, A full-core test method for experimental determination of convective-boiling heat transfer coefficients in tubes of cross-flow compact evaporators. In *Experimental Heat Transfer, Fluid Mechanics and Thermodynamics 1988* (Edited by R. K. Shah, E. N. Ganic and K. T. Yang), pp. 1473–1480 (1988).
5. V. P. Carey, T. Roddy and G. D. Mandrusiak, Analysis of heat transfer performance of offset strip fin geometries in a cold plate operating as part of a two-phase thermosyphon. In *Cooling Technology for Electronic Equipment* (Edited by W. Aung), pp. 95–112. Hemisphere, New York (1988).
6. G. F. Hewitt and D. N. Roberts, Studies of two-phase flow patterns by simultaneous X-ray and flash photography, AERE Report AERE-M-2159, HMSO (1969).
7. D. L. Bennett and J. C. Chen, Forced convective boiling in vertical tubes for saturated pure components and binary mixture, *A.I.Ch.E. Jl* **26,** 454–461 (1980).
8. V. P. Carey and G. D. Mandrusiak, Annular film-flow boiling of liquids in a partially heated vertical channel with offset strip fins, *Int. J. Heat Mass Transfer* **29,** 927–939 (1986).
9. J. G. Collier, Forced convective boiling. In *Two Phase Flow and Heat Transfer in the Power and Process Industries*, Chap. 8. Hemisphere, New York (1981).
10. G. D. Mandrusiak and V. P. Carey, Convective boiling in vertical channels with different offset strip-fin geometries, *ASME J. Heat Transfer* **111,** 156–165 (1989).

COMPARAISON DES CARACTERISTIQUES DE L'EBULLITION EN ECOULEMENT DANS DES CANAUX A STRIES TRANSVERSALES ET PARTIELLEMENT CHAUFFES, DE GEOMETRIES DIFFERENTES

Résumé—On rapporte les résultats de mesure locale de transfert thermique et de visualisation d'écoulement pour l'ébullition convective de R113 et de méthanol dans des canaux verticaux à stries transversales semblables aux géométries utilisées dans des échangeurs compacts à plaques. Des expériences sont conduites avec une section de mesure dans laquelle une paroi de canal est chauffée tandis que l'opposée est adiabatique et transparente pour permettre une visualisation de l'écoulement. Les données de transfert thermique sont obtenues pour trois configurations de stries différentes et des débits de réfrigérants compris entre 40 et 230 kg m^{-2} s^{-1} et les qualités entre 0,10 et 0,80. La comparaison des résultats avec ceux déjà rapportés pour une quatrième géométrie montre que les variations de l'espacement des nervures et de l'angle ont un effet sensible sur la performance du transfert de chaleur. La mise en rotation et l'agitation induites par les nervures augmentent le coefficient de transfert par ébullition convective d'un facteur 4 environ, par rapport au cas d'un tube circulaire dans des conditions d'écoulement comparable. On discute aussi des méthodes de corrélation des données de transfert thermique pour ces géométries et pour l'ébullition convective avec film annulaire.

VERGLEICH DER CHARAKTERISTIKA BEIM STRÖMUNGSSIEDEN IN TEILBEHEIZTEN QUERBERIPPTEN KANÄLEN MIT UNTERSCHIEDLICHER RIPPENGEOMETRIE

Zusammenfassung—Die gemessenen örtlichen Wärmeübergangskoeffizienten werden gemeinsam mit den Experimenten zur Strömungsvisualisierung beim konvektiven Sieden von R113 und Methanol in senkrechten querberippten Kanälen mit Geometrien ähnlich denen bei kompakten Plattenwärmetauschern dargestellt. Die Experimente werden in einer Meßstrecke durchgeführt, in der die eine Kanalwand beheizt wird, während die gegenüberliegende Wand adiabatisch und transparent ist, um gleichzeitig die Beobachtung der Strömung zu ermöglichen. Die Wärmeübergangskoeffizienten wurden für drei verschiedene Rippenformen bei Massenstromdichten zwischen 40 und 230 kg m^{-2} s^{-1} und Dampfgehalten zwischen 0,1 und 0,8 ermittelt. Der Vergleich dieser Ergebnisse mit denen einer vierten Geometrie, über die bereits früher berichtet wurde, zeigt, daß die Änderung des Rippenzwischenraums und -winkels einen wesentlichen Einfluß auf den Wärmeübergang beim Sieden hat. Die Änderung der Rippenform in diesen Kanälen zeigt nur einen schwachen Einfluß auf den Wärmeübergang. Die von den Rippen verursachten Wirbel und Störungen erhöhen den konvektiven Wärmeübergangskoeffizienten um ungefähr den Faktor vier gegenüber vergleichbaren Strömungsbedingungen in einem zylindrischen Rohr. Es werden außerdem Methoden zur Korrelation der Wärmeübergangskoeffizienten für das Sieden bei Ringströmung in diesen Geometrien erörtert.

СРАВНЕНИЕ ХАРАКТЕРИСТИК КИПЕНИЯ ПОТОКОВ В НАГРЕТЫХ КАНАЛАХ С ПОПЕРЕЧНЫМ ОРЕБРЕНИЕМ РАЗЛИЧНЫХ ГЕОМЕТРИЙ

Аннотация—Представлены данные измерений локального теплопереноса и результаты визуализации потока при конвективном кипении R-113 и метанола в вертикальных каналах с поперечным оребрением, геометрия которых аналогична используемой в компактных пластинчатых теплообменниках. Опыты проведены на участке, где одна стенка нагревается, а противоположная—адиабатична и прозрачна, что делает возможным визуализацию потока. Данные по теплопереносу получены для трех различных конфигураций оребрения в диапазонах значений массового потока хладагента 40–230 кг $м^{-2}$ $с^{-1}$ и массосодержания 0,10–0,80. Анализ этих данных, а также ранее опубликованных результатов для еще одной геометрии показывает, что изменения расстояний и углов между ребрами оказывают существенное влияние на характеристики теплопереноса при кипении. Найдено, что изменение конфигурации поперечного оребрения лишь незначительно влияет на теплоперенос. Обнаружено, что вызванные оребрением завихрение и перемешивание увеличивают коэффициент конвективного теплопереноса в случае кипения в 4 раза по сравнению с данными для круглой трубы при сопоставимых условиях течения. Обсуждаются также методы корреляции результатов по теплопереносу в случае кипения при пленочном кольцевом течении в тех же условиях.